

\mathcal{PT} -Symmetric Coherent Perfect Absorber with Graphene

Mustafa Sarisaman^{1*}

Department of Physics, Istanbul University, 34134 Istanbul, Turkey

Murat Tas^{2†}

Department of Physics, Gebze Technical University, 41400 Kocaeli, Turkey

We investigate \mathcal{PT} -symmetric coherent perfect absorbers (CPAs) in the TE mode solution of a linear homogeneous optical system surrounded by graphene sheets. It is revealed that presence of graphene sheets contributes the enhancement of absorption in a coherent perfect absorber. We derive exact analytic expressions, and work through their possible impacts on lasing threshold and CPA conditions. We point out roles of each parameter governing optical system with graphene and show that optimal conditions of these parameters give rise to enhancement and possible experimental realization of a CPA laser. Presence of graphene leads the required gain amount to reduce considerably based on its chemical potential and temperature. We obtain that relation between system parameters decides the measure of CPA condition. We find out that graphene features contributing to resonance effect in graphene sheets are rather preferable to build a better coherent perfect absorber.

Pacs numbers: 03.65.Nk, 42.25.Bs, 42.60.Da, 24.30.Gd

I. INTRODUCTION

The coherent perfect absorbers (CPAs), or antilasers, [1–8] are fascinating optical constructs that furnish in principle the absorption of certain incident coherent waves by the optical potential, but yet they basically act as a theoretical design today. Since they operate as time reversal case of regular lasers, they are inherently expressed by the time reversal symmetry of spectral singularities [9–13], which are used as a tool to render the best way of examining lasing threshold condition [14] in a laser. Thus, complex conjugate of the optical potential that supports a spectral singularity engenders a CPA-laser action [15]. Accordingly, it is intriguing to consider a \mathcal{PT} -symmetric potential that endorses both a spectral singularity and CPA concurrently. This is rather interesting because it functions as a laser emitting coherent waves unless it is subject to incident coherent waves with appropriate amplitude and phase in which case it acts as an absorber [16]. Although recent experimental realizations of CPAs have been carried out [17–19], basically they still stand as theoretical structures awaiting experimental advancement, see also [8] for a recent review of CPAs.

Since its debut, \mathcal{PT} symmetry has found considerable interest in optics and related fields due to its smoothness to realize experimental investigations and immediate applications. A generic \mathcal{PT} -symmetric Hamiltonian in optics is vested with a potential whose peculiar property is $V(x) = V^*(-x)$ [20–26], which corresponds to switching gain and loss components in conserved potential. Complex optical \mathcal{PT} -symmetric potentials are realized by the formal equivalence between quantum mechanical Schrödinger equation and optical wave equation derived from Maxwell equations. By exploiting optical modulation of the refractive index in the complex dielectric permittivity plane and engineering both optical absorption and amplification, \mathcal{PT} -symmetric optical systems can lead to a series of intriguing optical phenomena and devices, such as dynamic power oscillations of light propagation, CPA-lasers [16, 27–31], spectral singularities [9–13, 32–35] and unidirectional invisibility [20–24, 36–39].

Emergence of CPA-lasers is among the most notable applications of \mathcal{PT} -symmetric potentials in optics. In the context of \mathcal{PT} -symmetry, the condition for appearance of a spectral singularity coincides with that of its time-reversal [40]. This makes \mathcal{PT} -symmetric CPA-lasers as one of the primary examples in the study of \mathcal{PT} -symmetric optical structures [41]. This elegant finding motivates new insight towards solving the problem of constructing a CPA with appropriate amplitudes and phases of incoming waves. In view of this motivation, here we examine feasibility of realizing a CPA-laser in a homogeneous \mathcal{PT} -symmetric optical slab system covered by graphene sheets. Our aim in using the graphene sheets is to enhance the adjustment of absorption in entire system [42–47].

Physical properties of graphene has been profoundly unveiled and thus its numerous applications in condensed matter physics and optics have attracted interest of researchers for over a decade [48–51]. Since its early discovery,

*Electronic address: mustafa.sarisaman@istanbul.edu.tr

†Electronic address: tasm236@gmail.com

a voluminous literature has arisen and plenty of applications have been realized especially in the fields of sensor based transport phenomena [52–58], impurity invisibility [59], electron optics with p-n junctions [60], and invisibility cloaking [61–63]. The idea that graphene interact with electromagnetic waves in anomalous and exotic ways, providing new phenomena and applications, gives rise to the study of CPA phenomenon in \mathcal{PT} -symmetric optical structures with graphene. Especially recent works in this field [16, 42–47] fashion up essential motivation for this study, which will use whole competency of the transfer matrix method in a scattering formalism which grounds its power on Maxwell equations. Furthermore, see [64–67] for some relevant studies of graphene based light modulation and optical gain.

In a scattering problem the transfer matrix is used to encapsulate all the scattering data [68]. Its composition property makes it more practical and preferable than scattering matrix. Moreover, its components involve necessary information to reveal spectral singularities, CPA and invisibility of electromagnetic fields interacting with an optically active medium [16, 27–31]. See also [69–71] for the use of transfer matrix formalism belonging to the scattering of layered structures containing graphene.

Our analysis fulfils oblique incidence [16, 72], considering that desired phenomena may be angle dependent. Hence, we conduct a comprehensive study of spectral singularities which yields lasing threshold condition and CPAs in the oblique TE mode of a \mathcal{PT} -symmetric system with graphene to unveil the intriguing traits of transfer matrix as complementary to [16]. Our system is depicted in Fig. 1.

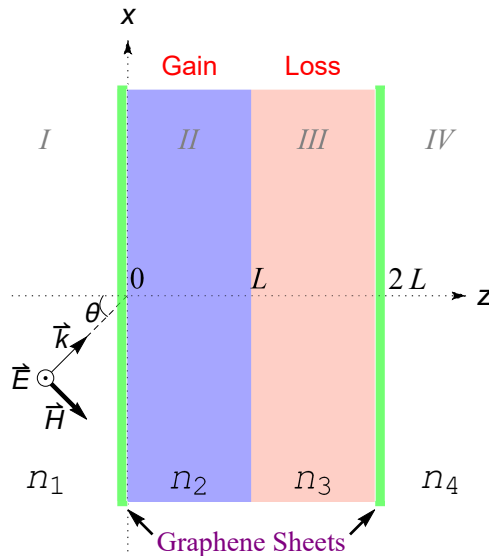


FIG. 1: (Color online) Diagram depicting the TE mode solution of parallel pair of slab system covered by graphene sheets in vacuum. Regions *II* and *III* with thickness L are respectively the gain and loss layers having refractive indices n_2 and n_3 . Regions *I* and *IV* correspond to the vacuum.

Our analysis demonstrates all possible configurations of the system leading to spectral singularity and CPA solutions. We find out complete solutions and schematically demonstrate their behaviors using various parameter choices. Among all possible parameters of the system which provide valuable information about the CPA-lasers, only optimal ones lead to achieve performing an efficient CPA. In particular, we obtain analytic expressions for the spectral singularity and CPA configurations, and examine behaviors of practically most desirable choices of parameters corresponding to TE waves. We reveal that optimal control of graphene parameters, such as gain coefficient, incidence angle, slab thickness, temperature, and chemical potential, gives rise to a desired outcome for achieving enhancement of absorption, and computing correct amplitude and phase contrasts in a CPA-laser. Thus, we provide a concrete ground that restrict the mentioned parameters of graphene in certain ranges. Optimal values of these parameters should be adjusted in a given system if one desires the experimental realization of CPA.

II. TE MODE SOLUTION OF A PLANAR BILAYER SLAB SYSTEM WITH GRAPHENES

Consider a one-dimensional linear homogeneous and optically active parallel pair of slab system whose exterior planar surfaces are covered by graphene layers as depicted in Fig. 1. Suppose that entire optical system is immersed in air and regions *II* and *III* are respectively filled with gain and loss materials having constant complex refractive

indices \mathbf{n}_2 and \mathbf{n}_3 . Let this system be exposed to external time harmonic electromagnetic waves with electric $\vec{\mathcal{E}}$ and magnetic $\vec{\mathcal{H}}$ fields. Maxwell equations describing interaction of the electromagnetic waves with the slab system have the form:

$$\vec{\nabla} \cdot \vec{\mathcal{D}}^j = \rho_j(z), \quad \vec{\nabla} \cdot \vec{\mathcal{B}}^j = 0, \quad (1)$$

$$\vec{\nabla} \times \vec{\mathcal{H}}^j - \partial_t \vec{\mathcal{D}}^j = \sigma_j(z) \vec{\mathcal{E}}^j, \quad \vec{\nabla} \times \vec{\mathcal{E}}^j + \partial_t \vec{\mathcal{B}}^j = 0, \quad (2)$$

where the index $j = 1, 2, 3, 4$ represents the regions sketched in Fig. 1, $\vec{\mathcal{E}}^j$ and $\vec{\mathcal{H}}^j$ are the electric and magnetic fields in corresponding regions. They are connected to $\vec{\mathcal{D}}^j$ and $\vec{\mathcal{B}}^j$ fields via the constitutive relations

$$\vec{\mathcal{D}}^j := \varepsilon_0 \mathfrak{z}_j(z) \vec{\mathcal{E}}^j, \quad \vec{\mathcal{B}}^j := \mu_0 \vec{\mathcal{H}}^j,$$

ε_0 and μ_0 are respectively the permeability and permittivity of the vacuum. We defined complex quantity $\mathfrak{z}_j(z)$

$$\mathfrak{z}_j(z) := \mathbf{n}_j \quad \text{for } z \in z_j, \quad (3)$$

such that the subindex $j = 1, 4$ correspond to vacuum at which $\mathbf{n}_1 = \mathbf{n}_4 = 1$, $j = 2, 3$ represent respectively the gain and loss components of the slab, and z_j stands for z coordinates in the specified j -th region as depicted in Fig. 1. In Maxwell equations (1) and (2), $\rho_j(z)$ and $\sigma_j(z)$ respectively denote the free charge and conductivity present on the graphene sheets and therefore expressed as

$$\begin{aligned} \rho_j(z) &:= \rho_g^{(1)} \delta(z) + \rho_g^{(2)} \delta(z - 2L), \\ \sigma_j(z) &:= \sigma_g^{(1)} \delta(z) + \sigma_g^{(2)} \delta(z - 2L), \end{aligned}$$

where $\rho_g^{(\ell)}$ and $\sigma_g^{(\ell)}$ are respectively the free charge and conductivity on the ℓ -th layer of graphene, with $\ell = 1, 2$. Notice that $\rho_j(z)$ and $\sigma_j(z)$ are associated to each other by the continuity equation

$$\vec{\nabla} \cdot \vec{\mathcal{J}}_j + \partial_t \rho_j(z) = 0 \quad (4)$$

for the electric current density $\vec{\mathcal{J}}_j := \sigma_j(z) \vec{\mathcal{E}}^j$. Conductivity of graphene sheets has been determined within the random phase approximation in [73–75] as the sum of intraband and interband contributions, i.e. $\sigma_g = \sigma_{intra} + \sigma_{inter}$, where

$$\begin{aligned} \sigma_{intra} &:= [ie^2 \chi / \pi \hbar^2 (\omega + i\Gamma)] \ln \left[2 \cosh \left(\frac{\mu}{\chi} \right) \right], \\ \sigma_{inter} &:= \frac{e^2}{4\pi \hbar} \left[\frac{\pi}{2} + \arctan \left(\frac{\nu_-}{\chi} \right) - \frac{i}{2} \ln \frac{\nu_+^2}{\nu_-^2 + \chi^2} \right]. \end{aligned} \quad (5)$$

Here $\nu_{\pm} := \hbar\omega \pm 2\mu$, $\chi := 2k_B T$, $-e$ is electron charge, \hbar is reduced Planck's constant, k_B is Boltzmann constant, T is temperature, Γ is the scattering rate of charge carriers, μ is the chemical potential, and $\hbar\omega$ is the photon energy [63]. In time harmonic forms, $\vec{\mathcal{E}}^j(\vec{r}, t)$ and $\vec{\mathcal{H}}^j(\vec{r}, t)$ fields are respectively given by $\vec{\mathcal{E}}^j(\vec{r}, t) = e^{-i\omega t} \vec{E}^j(\vec{r})$ and $\vec{\mathcal{H}}^j(\vec{r}, t) = e^{-i\omega t} \vec{H}^j(\vec{r})$. Thus, Maxwell equations corresponding to transverse electric (TE) wave solutions yield the following form of Helmholtz equation

$$[\nabla^2 + k^2 \mathfrak{z}_j(z)] \vec{E}^j(\vec{r}) = 0, \quad \vec{H}^j(\vec{r}) = -\frac{i}{kZ_0} \vec{\nabla} \times \vec{E}^j(\vec{r}), \quad (6)$$

where $\vec{r} := (x, y, z)$, $k := \omega/c$ is the wavenumber, $c := 1/\sqrt{\mu_0 \varepsilon_0}$ is the speed of light in vacuum, and $Z_0 := \sqrt{\mu_0/\varepsilon_0}$ is the impedance of vacuum. We stress out that TE waves correspond to the solutions of (6) for which $\vec{\mathcal{E}}^j(\vec{r})$ is parallel to the surface of the slabs. In our geometrical setup, they are aligned along the y -axis. Suppose that in region I , incident wave $\vec{E}^1(\vec{r})$ adapts a plane wave with wavevector \vec{k} in the x - z plane, specified by

$$\vec{k} = k_x \hat{e}_x + k_z \hat{e}_z, \quad k_x := k \sin \theta, \quad k_z := k \cos \theta, \quad (7)$$

where \hat{e}_x, \hat{e}_y , and \hat{e}_z , are respectively the unit vectors along the x -, y - and z -directions, and $\theta \in [-90^\circ, 90^\circ]$ is the incidence angle (See Fig. 1). For convenience we introduce the scaled variables

$$\mathbf{z} := \frac{z}{L}, \quad \mathbf{x} := \frac{x}{L}, \quad \mathfrak{K} := Lk_z = kL \cos \theta. \quad (8)$$

Thus, the electric field corresponding to TE waves is given by

$$\vec{E}^j(\vec{r}) = \mathcal{E}^j(L\mathbf{z})e^{i\mathfrak{K}\mathbf{x}\tan\theta\hat{e}_y}, \quad (9)$$

where \mathcal{E}^j is solution of the Schrödinger equation

$$-\psi^{j''}(\mathbf{z}) + v_j(\mathbf{z})\psi^j(\mathbf{z}) = \mathfrak{K}^2\psi^j(\mathbf{z}) \quad \mathbf{z} \notin \{0, 1, 2\}, \quad (10)$$

for the potential $v_j(\mathbf{z}) := \mathfrak{K}^2[1 - \tilde{\mathbf{n}}_j^2]$. Here we define $\tilde{\mathbf{n}}_j$

$$\tilde{\mathbf{n}}_j := \sec\theta\sqrt{\mathbf{n}_j^2 - \sin^2\theta}. \quad (11)$$

The fact that potential $v_j(\mathbf{z})$ is constant in regions of interest gives rise to a solution in relevant regions

$$\psi^j(\mathbf{z}) := a_j e^{i\mathfrak{K}_j\mathbf{z}} + b_j e^{-i\mathfrak{K}_j\mathbf{z}} \quad \text{for } \mathbf{z} \in \mathbf{z}_j, \quad (12)$$

where a_j and b_j , with $j = 1, 2, 3, 4$, are \mathfrak{K} -dependent complex coefficients, and

$$\mathfrak{K}_j := \mathfrak{K}\tilde{\mathbf{n}}_j. \quad (13)$$

In particular, $\mathcal{E}^j(L\mathbf{z})$ is given by the right-hand side of (12) with generally different choices of constants a_j and b_j . These coefficients are related to each other via appropriate boundary conditions: tangential components of \vec{E}^j and \vec{H}^j are continuous across the surface while the normal components of \vec{H}^j have a step of unbounded surface currents across the interface of graphenes. Table I displays corresponding set of boundary conditions. Quantities $\mathbf{u}_{\pm}^{(j)}$ are defined as

$$\mathbf{u}_{\pm}^{(j)} := \frac{1 \pm \sigma_g^{(j)}}{\tilde{\mathbf{n}}_j}. \quad (14)$$

$\mathbf{z} = 0$	$a_2 + b_2 = a_1 + b_1, \quad a_2 - b_2 = \mathbf{u}_+^{(2)}a_1 - \mathbf{u}_-^{(2)}b_1$
$\mathbf{z} = 1$	$a_2e^{i\mathfrak{K}_2} + b_2e^{-i\mathfrak{K}_2} = a_3e^{i\mathfrak{K}_3} + b_3e^{-i\mathfrak{K}_3}$ $\tilde{\mathbf{n}}_2(a_2e^{i\mathfrak{K}_2} - b_2e^{-i\mathfrak{K}_2}) = \tilde{\mathbf{n}}_3(a_3e^{i\mathfrak{K}_3} - b_3e^{-i\mathfrak{K}_3})$
$\mathbf{z} = 2$	$a_3e^{2i\mathfrak{K}_3} + b_3e^{-2i\mathfrak{K}_3} = a_4e^{2i\mathfrak{K}} + b_4e^{-2i\mathfrak{K}}$ $a_3e^{2i\mathfrak{K}_3} - b_3e^{-2i\mathfrak{K}_3} = \mathbf{u}_-^{(3)}a_4e^{2i\mathfrak{K}} - \mathbf{u}_+^{(3)}b_4e^{-2i\mathfrak{K}}$

TABLE I: Boundary conditions for TE waves.

III. TRANSFER MATRIX AND SPECTRAL SINGULARITIES

Right outgoing waves could be associated to the left ones by means of the transfer matrix. Transfer matrix is favored over the scattering matrix by virtue of its composition property, which helps being articulated the scattering properties of any optical system. For our two-layer optical system furnished by \mathcal{PT} -symmetry with graphene sheets, total transfer matrix can be obtained as the product of transfer matrices of gain and loss regions. If individual transfer matrices corresponding to the gain and loss regions of the slab are denoted by \mathbf{M}_1 and \mathbf{M}_2 respectively, then total transfer matrix $\mathbf{M} = [M_{ij}]$ satisfies composition property $\mathbf{M} = \mathbf{M}_2\mathbf{M}_1$, and is expressed by

$$\begin{bmatrix} a_4 \\ b_4 \end{bmatrix} = \mathbf{M} \begin{bmatrix} a_1 \\ b_1 \end{bmatrix}.$$

Spectral singularities match up to real zeros of M_{22} component of \mathbf{M} , which is computed explicitly as

$$M_{22} = \frac{e^{2i\mathfrak{K}}}{8} \left[V_+(\mathbf{u}_-^{(3)} - 1)e^{i\mathfrak{K}_3} + V_-(\mathbf{u}_-^{(3)} + 1)e^{-i\mathfrak{K}_3} \right], \quad (15)$$

where we identify

$$V_{\pm} := (\tilde{\mathbf{n}}_3 \pm \tilde{\mathbf{n}}_2)(1 - \mathbf{u}_{-}^{(2)})e^{i\tilde{\mathfrak{K}}_2} + (\tilde{\mathbf{n}}_3 \mp \tilde{\mathbf{n}}_2)(1 + \mathbf{u}_{-}^{(2)})e^{-i\tilde{\mathfrak{K}}_2}.$$

It is apparent that \mathcal{PT} -symmetry implies the following relations

$$\begin{aligned} \mathbf{n}_2 &\xleftrightarrow{\mathcal{PT}} \mathbf{n}_3, & \tilde{\mathbf{n}}_2 &\xleftrightarrow{\mathcal{PT}} \tilde{\mathbf{n}}_3, \\ \mathbf{u}_{\pm}^{(2)} &\xleftrightarrow{\mathcal{PT}} \mathbf{u}_{\mp}^{(3)}, & \sigma_g^{(2)} &\xleftrightarrow{\mathcal{PT}} -\sigma_g^{(3)}. \end{aligned} \quad (16)$$

Thus it amounts that currents on the left and right graphene sheets flow in opposite directions by virtue of \mathcal{PT} symmetry. Spectral singularities correspond to real values of the wavenumber k such that $M_{22} = 0$. Hence, (15) gives rise to explicit form of the spectral singularity condition

$$e^{2i\tilde{\mathfrak{K}}_3} = \frac{V_- (1 + \mathbf{u}_{-}^{(3)})}{V_+ (1 - \mathbf{u}_{-}^{(3)})}. \quad (17)$$

We note that quantities $\mathbf{u}_{-}^{(2,3)}$ involve the effect of graphene in the spectral singularities as given by identity (14). Provided that graphene layers are removed by setting $\sigma_g^{(2,3)} = 0$, (17) generates the spectral singularity condition given in [16].

IV. SPECTRAL SINGULARITIES IN \mathcal{PT} -SYMMETRIC CONFIGURATIONS

Spectral singularities corresponding to our optical setup in (17) describe the lasing threshold condition. This is in fact a complex expression screening behavior of system parameters. Thus, it can be explored in detail by means of relevant quantities containing significant physical consequences. In view of \mathcal{PT} symmetry relations given in (16), we obtain the following relations

$$\begin{aligned} \mathbf{n} &:= \mathbf{n}_2 = \mathbf{n}_3^*, & \tilde{\mathbf{n}} &:= \tilde{\mathbf{n}}_2 = \tilde{\mathbf{n}}_3^*, \\ \sigma_g &:= \sigma_g^{(2)} = -\sigma_g^{(3)*}, & \mathbf{u}_{\pm} &:= \mathbf{u}_{\pm}^{(2)} = \mathbf{u}_{\mp}^{(3)*}. \end{aligned} \quad (18)$$

Refractive index \mathbf{n} and $\tilde{\mathbf{n}}$ are expressed in real and imaginary parts as follows

$$\mathbf{n} = \eta + i\kappa, \quad \tilde{\mathbf{n}} = \tilde{\eta} + i\tilde{\kappa}. \quad (19)$$

Most of the materials safely satisfy the condition $|\kappa| \ll \eta - 1 < \eta$. In particular, this practical restriction of materials leads $\tilde{\eta}$ and $\tilde{\kappa}$ to be expressed in terms of η and leading order of κ as

$$\tilde{\eta} \approx \sec \theta \sqrt{\eta^2 - \sin^2 \theta}, \quad \tilde{\kappa} \approx \frac{\sec \theta \eta \kappa}{\sqrt{\eta^2 - \sin^2 \theta}}. \quad (20)$$

We next introduce the gain coefficient g and its threshold value g_0 at resonance frequency

$$g := -2k\kappa = -\frac{4\pi\kappa}{\lambda}, \quad g_0 := -2k_0\kappa_0 = -\frac{4\pi\kappa_0}{\lambda_0}, \quad (21)$$

where λ_0 corresponds to the resonance wavelength. In the light of (18), (19), (20) and (21), the spectral singularity condition (17) yields the following set of equations in the leading order of κ

$$2\tilde{\eta} \operatorname{Im}[\sigma_g] \sin(2\tilde{\mathfrak{K}}\tilde{\eta}) - 2\tilde{\eta}^2 \cos(2\tilde{\mathfrak{K}}\tilde{\eta}) = [e^{\tilde{g}L} - (\tilde{\eta} - \operatorname{Re}[\sigma_g])e^{-\tilde{g}L}] \tilde{\kappa} \operatorname{Im}[\sigma_g], \quad (22)$$

$$2 \left[\tilde{\eta}^2 + 1 - \operatorname{Re}[\sigma_g]^2 - \operatorname{Im}[\sigma_g]^2 \right] \sin(2\tilde{\mathfrak{K}}\tilde{\eta}) + 4 [\tilde{\eta} \operatorname{Im}[\sigma_g] - \tilde{\kappa} \operatorname{Re}[\sigma_g]] \cos(2\tilde{\mathfrak{K}}\tilde{\eta}) = \frac{\tilde{\kappa}}{\tilde{\eta}} (\mathbf{a}_- e^{-\tilde{g}L} - \mathbf{a}_+ e^{\tilde{g}L}), \quad (23)$$

where we define \mathbf{a}_{\pm} and \tilde{g} for convenience as follows

$$\begin{aligned} \mathbf{a}_{\pm} &:= \tilde{\eta}^2 - 1 \pm 2\tilde{\eta} \operatorname{Re}[\sigma_g] + \operatorname{Re}[\sigma_g]^2 + \operatorname{Im}[\sigma_g]^2, \\ \tilde{g} &:= \frac{\eta g}{\sqrt{\eta^2 - \sin^2 \theta}}. \end{aligned}$$

In practice, Eqs. (22) and (23) control the lasing behavior of our system in such a way that the most appropriate system parameters should be accounted for the emergence of optimal impacts. Graphene effect on the lasing occurrence is revealed by the presence of real and imaginary parts of σ_g . Thus, a comprehensive analysis of the involvement of system parameters is required to observe final outcome in the presence of graphene sheets. For this purpose we exhibit general behaviors of system parameters through the gain coefficient g plots. We employ Nd:YAG crystals in \mathcal{PT} -symmetric bilayer slab system with following specifications

$$\eta = 1.8217, \quad \lambda = 808 \text{ nm}, \quad L = 1 \text{ cm}, \quad \theta = 30^\circ, \quad (24)$$

and graphene sheets with characterizations

$$T = 300 \text{ }^\circ\text{K}, \quad \Gamma = 0.1 \text{ meV}, \quad \mu = 0.05 \text{ eV}. \quad (25)$$

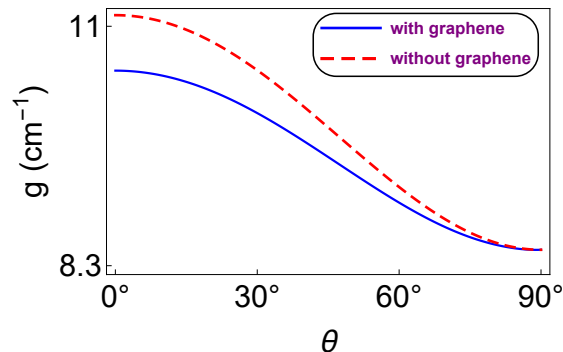


FIG. 2: (Color online) Behavior of gain amount g as a function of incidence angle θ in the cases of with and without graphene. We use parameter values given in (24) and (25) for our system. Gain amount runs short in the presence of graphene and retains a finite value in the limit of right angle incidence.

In Fig. 2, appearance of graphene sheets is distinguished in the plot of gain coefficient g as a function of incidence angle θ . We use the parameters as given in (24) for the slab, and in (25) for the graphene component. It is obvious that graphene triggers the gain value to reduce considerably, depending upon the properties of graphene sheets. As the incidence angle approaches to $\theta = 90^\circ$, graphene effect gets trivial and amount of the gain coefficient survives at a finite value as distinct from an individual layer case alone.

Figure 3 reflects essential behavior of curves in the plane of slab thickness L and gain g once the graphene sheets are inserted into the system. Gain values slightly drop off especially more at smaller thicknesses of micron sizes.

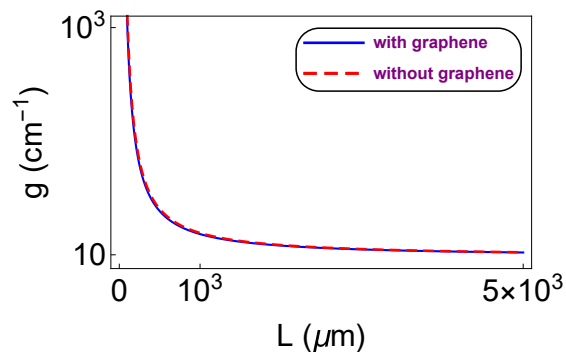


FIG. 3: (Color online) Gain value g as a function of slab thickness L when parameters of the system are given by (24) and (25). The required lasing gain amount slightly descends for smaller slabs, especially at micron sizes.

It turns out that characteristics of graphene layers manifest themselves in determining the rate of gain decrement. Fig. 4 displays attitudes of temperature and chemical potential of graphene sheets. It is revealed that optimal reduction of gain amount is achieved by employing as much lower temperatures and chemical potentials as possible. In particular, chemical potentials less than about $\mu = 3 \text{ meV}$ are favorable for the best effect. This is the case

$\mu \leq \hbar\omega/2$. Around the resonance of graphene where the relation $\mu = \hbar\omega/2$ holds, the required gain amount for lasing rises and then proceeds to decay to $g \approx 10.02 \text{ cm}^{-1}$ when $\mu \geq \hbar\omega/2$. Lastly, we remark that temperature (also chemical potential) dependence of the refractive indices is ignored safely since it yields a negligible effect (about 0.001%) within the temperature limits of interest [77, 78], which guarantees validity of our results.

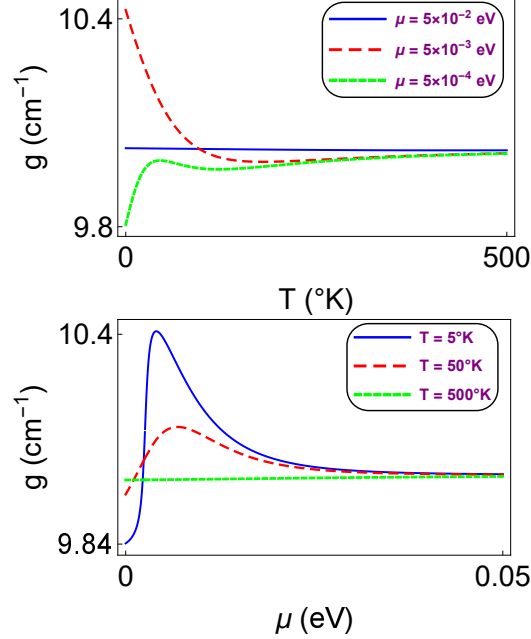


FIG. 4: (Color online) The roles of temperature and chemical potential of graphene sheets on the gain reduction. Temperatures around the absolute zero together with very small chemical potentials yield a large decrement in the gain coefficient.

V. PRESENCE OF DISPERSION CONTENT

We now assume that there exist a dispersion in the refractive index \mathbf{n} , and investigate its possible impacts on the spectral singularities. For this purpose, we include wavenumber k dependence of \mathbf{n} . We assume that active part of our optical system composing the gain ingredient is formed by doping a host medium of refractive index n_0 , and its refractive index satisfies the following dispersion relation

$$\mathbf{n}^2 = n_0^2 - \frac{\hat{\omega}_p^2}{\hat{\omega}^2 - 1 + i\hat{\gamma}\hat{\omega}}. \quad (26)$$

Here $\hat{\omega} := \omega/\omega_0$, $\hat{\gamma} := \gamma/\omega_0$, $\hat{\omega}_p := \omega_p/\omega_0$, ω_0 is the resonance frequency, γ is the damping coefficient, and ω_p is the plasmon frequency. The $\hat{\omega}_p^2$ can be described in leading order of the imaginary part κ_0 of \mathbf{n} at the resonance wavelength $\lambda_0 := 2\pi c/\omega_0$, by the expression $\hat{\omega}_p^2 = 2n_0\hat{\gamma}\kappa_0$ [76]. After inserting this relation into (26), employing the first expression of (19), and ignoring quadratic and higher order terms in κ_0 , we obtain the real and imaginary parts of the refractive index as [27–30]

$$\eta \approx n_0 + \frac{\kappa_0\hat{\gamma}(1 - \hat{\omega}^2)}{(1 - \hat{\omega}^2)^2 + \hat{\gamma}^2\hat{\omega}^2}, \quad \kappa \approx \frac{\kappa_0\hat{\gamma}^2\hat{\omega}}{(1 - \hat{\omega}^2)^2 + \hat{\gamma}^2\hat{\omega}^2}. \quad (27)$$

At resonance wavelength λ_0 , the κ_0 can be written as $\kappa_0 = -\lambda_0 g_0/4\pi$, see (21). Substituting this relation in (27) and making use of (19) and (17), we can determine λ and g_0 values for the spectral singularities. These are explicitly shown in the λ - g_0 plane in Fig. 5 for our setup with slab and graphene properties listed in (24) and (25), and for the incidence angle $\theta = 0^{\circ}$. Furthermore, Nd:YAG crystals which form the slab material hold the following $\hat{\gamma}$ value for given n_0 and λ_0 values [14]

$$n_0 = 1.8217, \quad \lambda_0 = 808 \text{ nm}, \quad \hat{\gamma} = 0.003094. \quad (28)$$

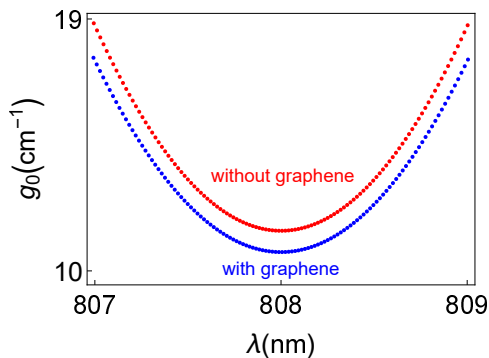


FIG. 5: (Color online) Threshold gain g_0 versus wavelength λ behavior corresponding to with and without graphene cases in the presence of dispersion. Apparently, g_0 has smaller values when the graphene sheets are inserted.

It appears that graphene sheets with associated parameters lead to shift down in the location of spectral singularity points. This verifies our findings explored in the previous section. Again at temperatures close to absolute zero and chemical potentials much lower values, the spectral singularity points move faster down in the λ - g_0 plane.

VI. CPA LASER ACTION

Our \mathcal{PT} -symmetric optical slab encrusted by graphene sheets serves as a CPA provided that time reversed system is fulfilled once the spectral singularities are prevalent. This phenomenon happens to exist only if correct phase and amplitude of incoming waves are originated. Thus, incoming waves are perfectly absorbed by the optical system that gives rise to a CPA-laser, see Fig. 6 for a pictorial demonstration of the phenomenon.

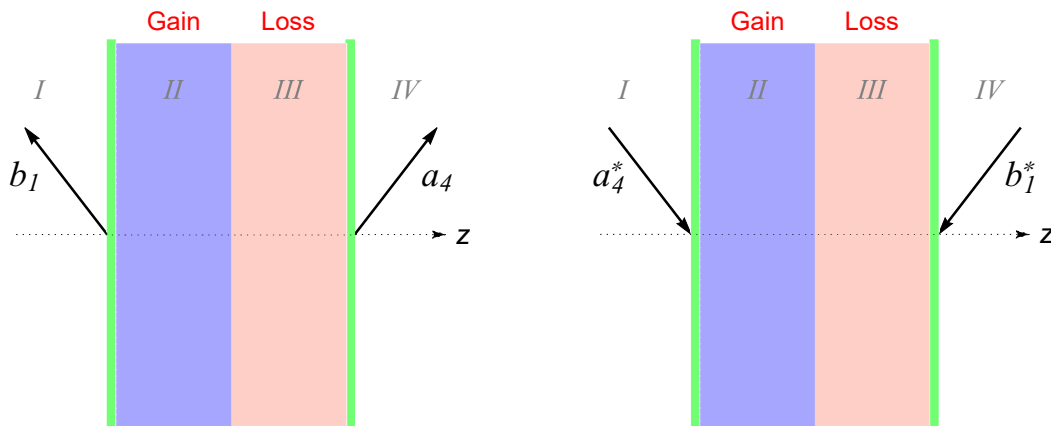


FIG. 6: (Color online) Configurations representing the spectral singularities (left plot), and coherent perfect absorber (CPA) (right plot). Spectral singularities correspond to purely outgoing waves while a CPA forms only when correct phases and amplitudes of incoming waves, as defined in Eqs. 31 and 32, are generated.

Spectral singularities displayed in the left panel of Fig. 6 describe purely outgoing waves. Time reversed case is just obtained by complex conjugation of waves outside the slab such that gain and loss parts are interchanged. To make a CPA-laser, we switch the gain and loss parts of time reversed case so that desired incoming waves can entirely be obtained as shown in the right panel of Fig. 6. For a required phenomena, waves outside the active part of the optical slab can be expressed as in Table II in terms of solutions of Maxwell equations in the exterior regions as given in (9) and (12).

CPA-laser operates once the incoming waves emergent by angle $-\theta$ are absorbed perfectly so that full destructive interference occurs. This can be measured by the ratio ρ of complex amplitude of incoming waves for $z \rightarrow 0$ and

	Spectrally Singular Waves	Time Reversed Waves	CPA Waves
Region I	$b_1 e^{i\tilde{\mathbf{R}}(\mathbf{x} \tan \theta - \mathbf{z})}$	$b_1^* e^{-i\tilde{\mathbf{R}}(\mathbf{x} \tan \theta - \mathbf{z})}$	$a_4^* e^{-2i\tilde{\mathbf{R}}} e^{-i\tilde{\mathbf{R}}(\mathbf{x} \tan \theta + \mathbf{z})}$
Region IV	$a_4 e^{i\tilde{\mathbf{R}}(\mathbf{x} \tan \theta + \mathbf{z})}$	$a_4^* e^{-i\tilde{\mathbf{R}}(\mathbf{x} \tan \theta + \mathbf{z})}$	$b_1^* e^{2i\tilde{\mathbf{R}}} e^{-i\tilde{\mathbf{R}}(\mathbf{x} \tan \theta - \mathbf{z})}$

TABLE II: Waves outside the \mathcal{PT} -symmetric optical slab with graphene corresponding to phenomena specified in the first row.

$z \rightarrow 2L$. In view of amplitudes given in Table II, this is expressed as

$$\rho = \frac{a_4^* e^{-2i\tilde{\mathbf{R}}}}{b_1^*}. \quad (29)$$

In fact, a_4 can be denominated in terms of b_1 by employing the spectral singularity condition. We recall that spectral singularities correspond to purely outgoing waves such that

$$a_1 = b_4 = 0.$$

This, together with the boundary conditions in Table I and spectral singularity condition in (17), leads to

$$a_4 = \frac{e^{-2i\tilde{\mathbf{R}}} b_1}{\tilde{\mathbf{n}}^*} \sqrt{\frac{V_+ V_-^*}{[1 + \mathbf{u}_+] [1 - \mathbf{u}_+]}}. \quad (30)$$

Thus, it is easy to show that incoming waves are perfectly absorbed provided that ratio of incoming amplitudes specified by ρ satisfies

$$\rho = \frac{1}{\tilde{\mathbf{n}}} \sqrt{\frac{V_+^* V_-}{[1 + \mathbf{u}_+] [1 - \mathbf{u}_+^*]}}. \quad (31)$$

Hence, ratio of amplitudes and phase factors of the waves incoming from left- and right-hand sides are characterized by $|\rho|$ and $\delta\phi$ respectively, and the latter is quantified as

$$e^{i\delta\phi} = \frac{\rho}{|\rho|}. \quad (32)$$

Consequently, the CPA-laser action can outrightly be obtained once the $|\rho|$ and $\delta\phi$ of incoming waves from the left and right-hand sides are tuned in according to expressions (31) and (32) respectively. Pictorial representation of how these quantities are influenced by parameters of the optical system are clearly shown in Figs. 7, 8 and 9. Note that in these figures the parameters assume the values given in (24) and (25).

Figure 7 displays dependence of $|\rho|$ and $\delta\phi$ on incidence angle θ . We set the gain amount to $g = 10 \text{ cm}^{-1}$, $\lambda = 808 \text{ nm}$, and $\mu = 5 \text{ meV}$. We notice that $|\rho|$ and $\delta\phi$ oscillate with angle θ such that peaks in the presence of graphene case slightly shift with respect to without graphene case, especially for small incidence angles, and they almost coincide for large incidence angles. It is obvious that presence of graphene requires larger $|\rho|$ compared to without graphene case for small and moderate incidence angles, and this influence decreases as θ gets larger. This means that amplitude of wave coming from the left side should be adjusted to have a little higher value compared to the amplitude of waves coming from the right side. In a similar manner, phase difference factor $\delta\phi$ for graphene shifts slightly, and could get any value for small incidence angles, and graphene induces this phase difference to rise significantly as the incidence angle increases. This amounts to that graphene mostly yields almost destructive interference. Graphene effect is not felt much for the angles close to right angles. See the last row of Fig. 7 for overall view of incidence angle dependence.

In Figs. 8 and 9, one explicitly realizes the effect of graphene for obtaining a CPA-laser. We employ the incidence angle $\theta = -30^\circ$, gain value $g = 10 \text{ cm}^{-1}$, and wavelength $\lambda = 808 \text{ nm}$. Figure 8 demonstrates how chemical potential variation of graphene sheets impacts on the ratio of amplitudes $|\rho|$ and phase difference $\delta\phi$ corresponding to different temperatures. We observe that chemical potentials less than about $\mu = 5 \text{ meV}$ give more $|\rho|$ and relatively small phase difference, especially at smaller temperatures. When μ increases till about 0.028 eV , the $|\rho|$ decreases and $\delta\phi$ increases. The point $\mu \approx 0.028 \text{ eV}$ corresponds to resonance value of graphene so that it is felt at small temperatures as noticed in the figure. When chemical potential gets values higher than $\mu = 0.028 \text{ eV}$, $|\rho|$ starts to scale up to get asymptotic value of about $|\rho| \approx 1.4$ while $\delta\phi$ reduces to get a value around $\delta\phi \approx 118^\circ$. These findings are verified in Fig. 9, i.e. the effect of graphene is perceived at considerably small temperatures, and temperatures giving rise to the resonance effect particularly for small chemical potentials such that $|\rho|$ increases whereas $\delta\phi$ decreases as temperature

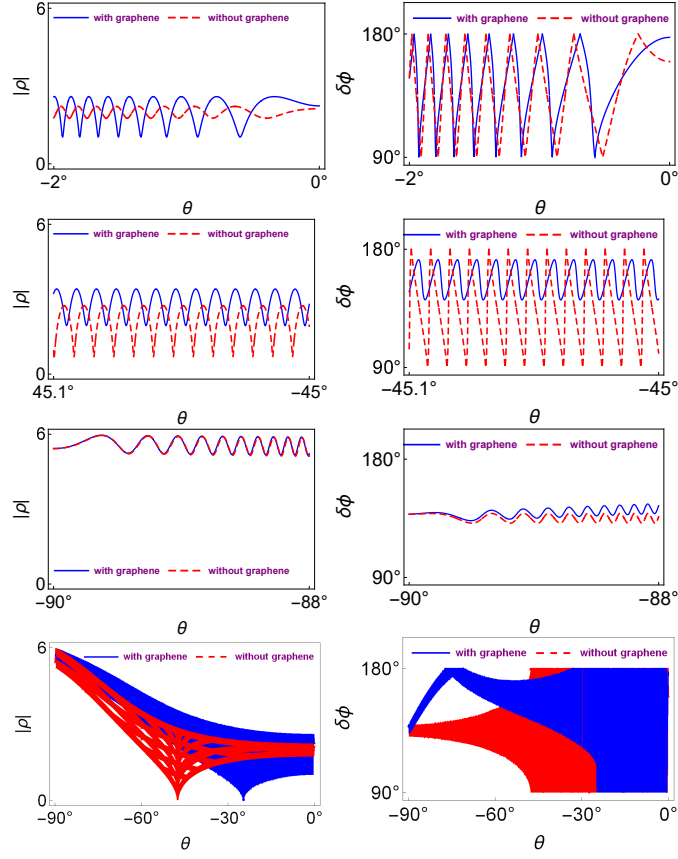


FIG. 7: (Color online) Dependence of $|\rho|$ and $\delta\phi$ on incidence angle θ in a system with and without graphene. System parameters are taken as in (24) and (25). Notice that presence of graphene results in larger $|\rho|$ and $\delta\phi$ depending on the θ .

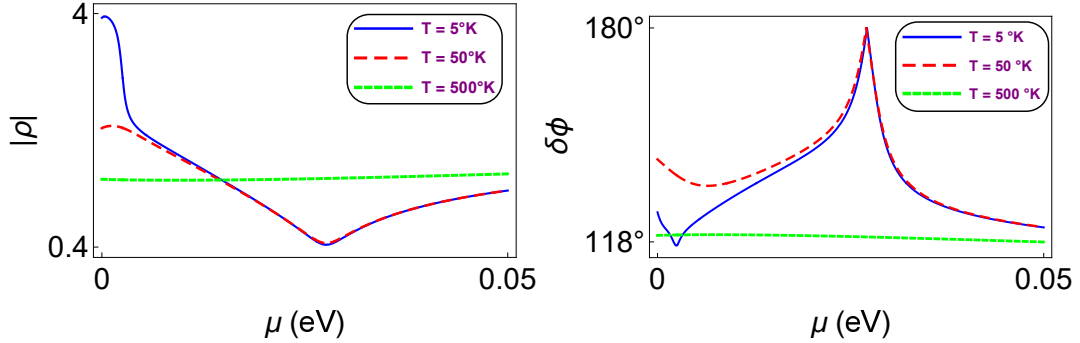


FIG. 8: (Color online) Conditions for obtaining a CPA-laser on how to tune the chemical potential of graphene at various temperatures. Incidence angle is opted for $\theta = -30^\circ$. Graphene manifests itself at very small μ values. Increasing temperature leads $|\rho|$ to move down, and $\delta\phi$ to move up at constant μ .

decreases from $T = 50^\circ\text{K}$, and $|\rho|$ decreases to minimum value and $\delta\phi$ increases to maximum value in temperature range $50^\circ\text{K} \lesssim T \lesssim 220^\circ\text{K}$. It is understood that temperature and chemical potential values close to resonance effect of graphene are favorable in order to get a well-adjusted CPA-laser.

Table III demonstrates some parameter values belonging to our optical system with and without graphene to realize a CPA-laser as an instructive guide for the experimental attempts. Properties of graphene sheets are specified by temperature $T = 300^\circ\text{K}$, chemical potential of $\mu = 0.05$ eV and $\Gamma = 0.1$ meV. Table IV explicitly presents values necessary to build a graphene based CPA-laser corresponding to graphene parameter values $T = 50^\circ\text{K}$ and

$\mu = 0.027$ eV (left board), and $T = 200$ °K and $\mu = 0.5$ eV (right board).

	with Graphene			–	without Graphene		
θ	0°	-40°	-80°		0°	-40°	-80°
λ	807.996 nm	808.008 nm	807.993 nm		808.006 nm	808.001 nm	808.009 nm
g	10.859 cm^{-1}	10.104 cm^{-1}	9.002 cm^{-1}		11.433 cm^{-1}	10.458 cm^{-1}	9.025 cm^{-1}
κ	-6.982×10^{-5}	-6.496×10^{-5}	-5.788×10^{-5}		-7.351×10^{-5}	-6.724×10^{-5}	-5.803×10^{-5}
$ \rho $	1.9053	1.8883	1.7817		0.5824	0.7597	1.5929
$\delta\phi$	146.106°	148.620°	179.940°		135.008°	135.007°	135.004°

TABLE III: Physical parameters of a CPA construct for various incidence angles corresponding to with and without graphene cases. Here graphene has $T = 300$ °K, $\mu = 0.05$ eV, and $\Gamma = 0.1$ meV.

	$T = 50^\circ$ and $\mu = 0.027$ eV			–	$T = 200^\circ$ and $\mu = 0.0005$ eV		
θ	0°	-40°	-80°		0°	-40°	-80°
λ	807.995 nm	808.007 nm	807.991 nm		807.994 nm	808.007 nm	807.991 nm
g	10.872 cm^{-1}	10.119 cm^{-1}	9.014 cm^{-1}		10.819 cm^{-1}	10.064 cm^{-1}	8.971 cm^{-1}
κ	-6.990×10^{-5}	-6.506×10^{-5}	-5.796×10^{-5}		-6.956×10^{-5}	-6.471×10^{-5}	-5.768×10^{-5}
$ \rho $	1.6713	1.6324	1.6591		1.6291	1.5982	1.6632
$\delta\phi$	157.613°	162.139°	160.031°		153.293°	158.044°	160.507°

TABLE IV: Physical parameters of a graphene-based CPA for various incidence angles. Here, graphene parameters are $T = 50$ °K, $\mu = 0.027$ eV, and $T = 200$ °K, $\mu = 0.5$ meV respectively. Scattering rate is taken as $\Gamma = 0.1$ meV.

VII. CONCLUDING REMARKS

This study benefits the idea that a CPA-laser is the time reversal construct of a regular laser which could be expressed by means of the spectral singularities. Nowadays, experimental realization of CPA-lasers is the main challenge due to difficulties in adjusting exact amplitude and phase factors of incoming waves. Current studies exploit various techniques in order to measure the quantities pointing CPA actions. In this work, we employed an optical system which respects the property of \mathcal{PT} -symmetry accompanied by graphene containment. In [16], necessary and sufficient conditions for implementing a CPA-laser based on the feature of \mathcal{PT} -symmetry are given, and in this current study we performed a comprehensive analysis aiming to find the conditions for CPA-laser action based on graphene sheets. Hence, the results of this study guide experimental attempts for realization of \mathcal{PT} -symmetric CPA phenomenon with graphene.

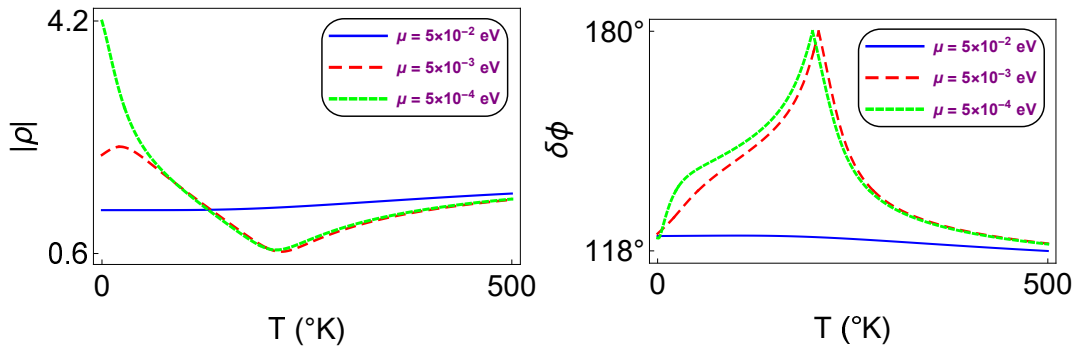


FIG. 9: (Color online) Impact of graphene temperature on $|\rho|$ and $\delta\phi$ necessary for obtaining a CPA-laser. Incidence angle is set to $\theta = -30^\circ$. Temperatures close to resonance values $T \approx 220$ °K together with small μ values are favorable if one desires to feel the presence of graphene in a CPA-laser.

We made use of distinctive traits of the transfer matrix formalism and determined the spectral singularities, which give rise to lasing threshold condition reflecting the presence of graphene in a \mathcal{PT} -symmetric optical system. The transfer matrix approach grounds the power of boundary conditions arising from the solutions coming directly from Maxwell equations. Table I reveals the presence of graphene sheets in boundary conditions in the form of complex function $\mathbf{u}_{\pm}^{(j)}$, see Eq. (14). We derived exact expressions for the conditions of lasing threshold in (17) and of coherent perfect absorber in (31) and (32). We employ a perturbative approach to obtain optimal conditions arising from the system parameters.

We require that graphene coatings respect overall \mathcal{PT} symmetry which leads to formation of currents flowing in opposite directions. We emphasize that \mathcal{PT} symmetry enables the emergence of lasing and CPA conditions due to its power to control the system parameters as distinct from non- \mathcal{PT} -symmetric structures. In particular, we find out that graphene insertion into a \mathcal{PT} -symmetric optical system leads lower gain values depending upon the graphene features, especially temperature and chemical potential. At this point, resonance occurrence of graphene plays a significant role which happens to exist at $\mu_r \approx 2.56$ meV at absolute zero temperature, and slightly shifts up with increasing temperature. In general, below the resonance point, the lower temperature and chemical potential of graphene sheets are, the less gain amount is. The results of spectral singularities and in turn lasing threshold conditions facilitate the path towards obtaining a CPA because of coincidence of both phenomena at the same points.

We observe that efficiency of a CPA-laser could be improved once the parameters of the optical system together with graphene features are well-adjusted. We consider \mathcal{PT} -symmetry to achieve computational and thus experimental accessibility of the optical system by tuning appropriate parameters of the system. Accordingly, we place graphene sheets at the ends of \mathcal{PT} -symmetric slab system just to realize that optimal conditions for the CPA-laser action can be obtained by computing appropriate intensity and phase contrasts. In order to get a lower intensity and higher phase contrast that yield an almost destructive interference, one should opt for lower temperatures and chemical potentials for the graphene sheets at which the resonance effect occurs. Also, small incidence angles provide relatively lower intensities in the presence of graphene, which lead to larger phase difference as desired. This is the main reason to use graphene sheets in the optical system.

In view of our findings, one can shape a reliable CPA equipment provided that parameters specifying the graphene and bilayer slab system are well-adjusted. In Tables III and IV we provide explicit values of parameters in order to build a concrete CPA. Our primary purpose in placing graphene is to improve absorption of waves and utilize arrangement of parameters. We explored that this is achieved at values especially around the resonance effect of graphene. Furthermore, it is observed that graphene causes the necessary gain amount to lessen. In this respect, we infer that presence of graphene gives valuable information about enhancement of absorption in a CPA, which helps building a better CPA. This suggests even a more effective material could be used instead of graphene to make a unity ratio of amplitudes and smooth phase contrast to make a perfect destructive interference. In this direction recently some prominent candidates have been intensely studied like Weyl semimetals may be in the limelight to build a better CPA.

As a final note, it would be interesting to describe the role of surface plasmon polaritons (SPPs) in our system. But, no surface modes should exist at the interface between the slab and graphene since we focused on TE polarization solutions. SPPs exist only for TM polarization. [79].

-
- [1] Y. D. Chong, L. Ge, H. Cao, and A. D. Stone, "Coherent perfect absorbers: time-reversed lasers," *Phys. Rev. Lett.* **105**, 053901 (2010).
 - [2] S. Longhi, "Backward lasing yields a perfect absorber," *Physics* **3**, 61 (2010).
 - [3] S. Longhi, " \mathcal{PT} -symmetric laser absorber," *Phys. Rev. A* **82**, 031801 (2010).
 - [4] S. Longhi, "Coherent perfect absorption in a homogeneously broadened two-level medium," *Phys. Rev. A* **83**, 055804 (2011).
 - [5] S. Longhi, "Time-Reversed Optical Parametric Oscillation," *Phys. Rev. Lett.* **107**, 033901 (2011).
 - [6] W. Wan, Y. Chong, L. Ge, H. Noh, A. D. Stone, and H. Cao, "Time-reversed lasing and interferometric control of absorption," *Science* **331**, 889 (2011).
 - [7] L. Ge, Y. D. Chong, S. Rotter, H. E. Türeci, and A. D. Stone, "Unconventional modes in lasers with spatially varying gain and loss," *Phys. Rev. A* **84**, 023820 (2011).
 - [8] D. G. Baranov, A. E. Krasnok, T. Shegai, A. Alù, and Y. D. Chong, "Coherent Perfect Absorbers: Advanced Structures for Linear Control of Light with Light," *Nat. Rev. Mater.* **2**, 17064 (2017).
 - [9] M. A. Naimark, "Investigation of the spectrum and the expansion in eigenfunctions of a nonselfadjoint differential operator of the second order on a semi-axis," *Trudy Moscov. Mat. Obsc.* **3**, 181 (1954) in Russian, English translation: *Amer. Math. Soc. Transl.* (2), **16**, 103 (1960).

- [10] G. Sh. Guseinov, "On the concept of spectral singularities," *Pramana J. Phys.* **73**, 587 (2009).
- [11] B. F. Samsonov, "Spectral singularities of non-Hermitian Hamiltonians and SUSY transformations," *J. Phys. A* **38**, L571 (2005).
- [12] A. Mostafazadeh, "Delta-function potential with a complex coupling," *J. Phys. A* **39**, 13495 (2006).
- [13] A. Mostafazadeh and H. Mehri-Dehnavi, "Spectral singularities, biorthonormal systems and a two-parameter family of complex point interactions," *J. Phys. A* **42**, 125303 (2009).
- [14] W. T. Silfvast, *Laser Fundamentals*, Cambridge University Press, Cambridge, 1996.
- [15] A. Mostafazadeh, "Self-dual spectral singularities and coherent perfect absorbing lasers without \mathcal{PT} -symmetry," *J. Phys. A* **45**, 444024 (2012).
- [16] A. Mostafazadeh and M. Sarisaman, "Spectral Singularities in the TE and TM modes of a \mathcal{PT} -Symmetric Slab System: Optimal conditions for realizing a CPA-Laser," *Ann. Phys.* **375**, 265 (2016).
- [17] S. Li, Q. Duan, S. Li, Q. Yin, W. Lu, L. Li, B. Gu, B. Hou and W. Wen, "Perfect electromagnetic absorption at one-atom-thick scale," *Appl. Phys. Lett.* **107**, 181112 (2015).
- [18] G. Pirruccio, L. M. Moreno, G. Lozano and J. G. Rivas, "Coherent and Broadband Enhanced Optical Absorption in Graphene," *ACS Nano* **7(6)**, 4810 (2013).
- [19] Z. J. Wong, Y. L. Xu, J. Kim, K. O'Brien, Y. Wang, L. Feng and X. Zhang, "Lasing and anti-lasing in a single cavity," *Nat. Photonics* **10**, 796 (2016).
- [20] C. M. Bender and S. Boettcher, "Real Spectra in Non-Hermitian Hamiltonians Having \mathcal{PT} Symmetry," *Phys. Rev. Lett.* **80** 5243, (1998).
- [21] C. M. Bender, D. C. Brody, and H. F. Jones, "Complex Extension of Quantum Mechanics," *Phys. Rev. Lett.* **89** 270401, (2001).
- [22] K. G. Makris, R. El-Ganainy, D. N. Christodoulides, and Z. H. Musslimani, "Beam Dynamics in \mathcal{PT} Symmetric Optical Lattices," *Phys. Rev. Lett.* **100** 103904, (2008).
- [23] A. Guo, G. J. Salamo, D. Duchesne, R. Morandotti, M. Volatier-Ravat, V. Aimez, G. A. Siviloglou, and D. N. Christodoulides, "Observation of \mathcal{PT} -Symmetry Breaking in Complex Optical Potentials," *Phys. Rev. Lett.* **103** 093902, (2009).
- [24] C. E. Rüter, K. G. Makris, R. El-Ganainy, D. N. Christodoulides, M. Segev, and D. Kip, "Observation of parity-time symmetry in optics," *Nat. Phys.* **6** 192, (2010).
- [25] L. Chen, R. Li, N. Yang, D. Chen, L. Li, "Optical modes in PT-symmetric double-channel waveguides," *Proc. Rom. Acad. Ser. A: Math. Phys. Tech. Sci. Inf. Sci.* **13**, 46 (2012).
- [26] R. Li, P. Li, L. Li, "Asymmetric optical amplifier based on parity-time symmetry," *Proc. Rom. Acad. A* **14**, 121 (2013).
- [27] A. Mostafazadeh, M. Sarisaman, "Spectral singularities of a complex spherical barrier potential and their optical realization," *Phys. Lett. A* **375**, 3387 (2011).
- [28] A. Mostafazadeh, M. Sarisaman, "Optical spectral singularities and coherent perfect absorption in a two-layer spherical medium," *Proc. R. Soc. Lond. Ser. A: Math. Phys. Eng. Sci.* **468**, 3224 (2012).
- [29] A. Mostafazadeh, M. Sarisaman, "Spectral singularities and whispering gallery modes of a cylindrical gain medium," *Phys. Rev. A* **87**, 063834 (2013).
- [30] A. Mostafazadeh, M. Sarisaman, "Spectral singularities in the surface modes of a spherical gain medium," *Phys. Rev. A* **88**, 033810 (2013).
- [31] A. Mostafazadeh and M. Sarisaman, "Lasing-threshold condition for oblique TE and TM modes, spectral singularities, and coherent perfect absorption," *Phys. Rev. A* **91**, 043804 (2015).
- [32] A. Mostafazadeh, "Physics of Spectral Singularities," *Geometric Methods in Physics, Trends in Mathematics*, edited by P. Kielanowski, P. Bieliavsky, A. Odziejewicz, M. Schlichenmaier, and T. Voronov (Springer, Cham, 2015) pp 145-165; arXiv: 1412.0454.
- [33] A. Mostafazadeh, "Invisibility and \mathcal{PT} symmetry," *Phys. Rev. A* **87**, 012103 (2013).
- [34] S. Longhi, "Invisibility in non-Hermitian tight-binding lattices," *Phys. Rev. A* **82**, 032111 (2010).
- [35] S. Longhi, "Invisibility in \mathcal{PT} -symmetric complex crystals," *J. Phys. A* **44**, 485302 (2011).
- [36] L. Feng, Y. L. Xu, W. S. Fegadolli, M. H. Lu, J. E. Oliveira, V. R. Almeida, Y. F. Chen, A. Scherer, "Experimental demonstration of a unidirectional reflectionless parity-time metamaterial at optical frequencies," *Nat. Mater.* **12**, 108 (2013).
- [37] Y. Shen, X. Hua Deng, and L. Chen, "Unidirectional invisibility in a two-layer non-PT-symmetric slab," *Opt. Express* **22**, 19440 (2014).
- [38] M. Sarisaman, "Unidirectional reflectionlessness and invisibility in the TE and TM modes of a \mathcal{PT} -symmetric slab system," *Phys. Rev. A* **95**, 013806 (2017).
- [39] M. Sarisaman, M. Tas, "Unidirectional invisibility and \mathcal{PT} symmetry with graphene," *Phys. Rev. B* **97**, 045409 (2018).
- [40] S. Longhi, "PT-symmetric laser absorber," *Phys. Rev. A* **82**, 031801 (2010).
- [41] A. Mostafazadeh, "Self-dual spectral singularities and coherent perfect absorbing lasers without \mathcal{PT} -symmetry," *J. Phys. A* **45**, 444024 (2012).
- [42] S. Zanotto, F. Bianco, V. Miseikis, D. Convertino, C. Coletti, and A. Tredicucci, "Coherent absorption of light by graphene and other optically conducting surfaces in realistic on-substrate configurations," *APL Photonics* **2**, 016101 (2017).
- [43] F. Liu, Y. D. Chong, S. Adam, M. Polini, "Gate-tunable coherent perfect absorption of terahertz radiation in graphene," *2D Mater.* **1**, 031001 (2014).
- [44] Y. Fan, F. Zhang, Q. Zhao, Z. Wei, and H. Li, "Tunable terahertz coherent perfect absorption in a monolayer graphene," *Opt. Lett.* **38**, 6269 (2014).

- [45] S. M. Rao, J. J. F. Heitz, T. Roger, N. Westerberg, and D. Faccio, "Coherent control of light interaction with graphene," *Opt. Lett.* **39**, 5345 (2014).
- [46] Y. Fan, Z. Liu, F. Zhang, Q. Zhao, Q. Fu, J. Li, C. Gu, and H. Li, "Tunable mid-infrared coherent perfect absorption in a graphene meta-surface," *Sci. Rep.* **5**, 13956 (2015).
- [47] J. Wang and X. Hu, "Recent Advances in Graphene-Assisted Nonlinear Optical Signal Processing," *J. of Nanotech.* **2016**, 7031913 (2016).
- [48] A. K. Geim and K. S. Novoselov, "The rise of graphene," *Nat. Mater.* **6**, 183 (2007).
- [49] A. K. Geim, "Graphene: Status and Prospects," *Science* **324**, 1530 (2009).
- [50] A. H. Castro Neto, F. Guinea, N. M. R. Peres, K. S. Novoselov, and A. K. Geim, "The electronic properties of graphene," *Rev. Mod. Phys.* **81**, 109 (2009).
- [51] O. V. Yazyev, "Emergence of magnetism in graphene materials and nanostructures," *Rep. Progr. Phys.* **73**, 056501 (2010).
- [52] F. Schedin, A. K. Geim, S. V. Morozov, E. W. Hill, P. Blake, M. I. Katsnelson, and K. S. Novoselov, "Detection of individual gas molecules adsorbed on graphene," *Nat. Mater.* **6**, 652 (2007).
- [53] R. Stine, J. T. Robinson, P. E. Sheehan, and Cy R. Tamanaha, "Real-Time DNA Detection Using Reduced Graphene Oxide Field Effect Transistors," *Adv. Mater.* **22**, 5297 (2010).
- [54] G. Lu, L. E. Ocola, and J. Chen, "Gas detection using low-temperature reduced graphene oxide sheets," *App. Phys. Lett.* **94**, 083111 (2009).
- [55] J. T. Robinson, F. K. Perkins, E. S. Snow, Z. Wei, and P. E. Sheehan, "Reduced Graphene Oxide Molecular Sensors," *Nano Lett.* **8**, 3137 (2008).
- [56] Y. Shao, J. Wang, H. Wu, J. Liu, I. A. Aksay, and Y. Lin, "Graphene Based Electrochemical Sensors and Biosensors: A Review," *Electroanalysis* **22**, 1027 (2010).
- [57] Q. He, S. Wu, Z. Yin, and H. Zhang, "Graphene-based electronic sensors," *Chem. Sci.* **3**, 1764 (2012).
- [58] S. Wu, Q. He, C. Tan, Y. Wang, and H. Zhang, "Graphene-Based Electrochemical Sensors," *Small* **9**, 1160 (2013).
- [59] J. Duffy, J. Lawlor, C. Lewenkopf, and M. S. Ferreira, "Impurity invisibility in graphene: Symmetry guidelines for the design of efficient sensors," *Phys. Rev. B* **94**, 045417 (2016).
- [60] S. Chen, Z. Han, M. M. Elahi, K. M. M. Habib, L. Wang, B. Wen, Y. Gao, T. Taniguchi, K. Watanabe, J. Hone, A. W. Ghosh, and C. R. Dean, "Electron optics with p-n junctions in ballistic graphene," *Science* **353**, 1522 (2016).
- [61] P. -Y. Chen and A. Alu, "Atomically Thin Surface Cloak Using Graphene Monolayers," *ACS Nano* **5**, 5855 (2011).
- [62] M. Danaeifar and N. Granpayeh, "Wideband invisibility by using inhomogeneous metasurfaces of graphene nanodisks in the infrared regime," *J. Opt. Soc. Am. B* **33**, 1764 (2016).
- [63] M. Naserpour, C. J. Zapata-Rodríguez, S. M. Vuković, H. Pashaeiadi and M. R. Belić, "Tunable invisibility cloaking by using isolated graphene-coated nanowires and dimers," *Sci. Rep.* **7**, 12186 (2017).
- [64] T. Low and P. Avouris, "Graphene Plasmonics for Terahertz to Mid-Infrared Applications," *ACS Nano* **8**, 1086 (2014).
- [65] Y. Fan, N. Shen, F. Zhang, Z. Wei, H. Li, Q. Zhao, Q. Fu, P. Zhang, T. Koschny, and C. M. Soukoulis, "Electrically Tunable Goos-Hänchen Effect with Graphene in the Terahertz Regime," *Adv. Opt. Mater.* **4**, 1824 (2016).
- [66] Y. Fan, N. Shen, T. Koschny, and C. Soukoulis, "Tunable Terahertz Meta-Surface with Graphene Cut-Wires," *ACS Photonics* **2**, 151 (2015).
- [67] Y. Fan, N. Shen, F. Zhang, Q. Zhao, Z. Wei, P. Zhang, J. Dong, Q. Fu, H. Li, and C. M. Soukoulis, "Photoexcited Graphene Metasurfaces: Significantly Enhanced and Tunable Magnetic Resonances," *ACS Photonics* **5**, 1612 (2018).
- [68] A. Mostafazadeh, "Spectral Singularities of Complex Scattering Potentials and Infinite Reflection and Transmission Coefficients at Real Energies," *Phys. Rev. Lett.* **102**, 220402 (2009).
- [69] T. Zhan, X. Shi, Y. Dai, X. Liu and J. Zi, "Transfer matrix method for optics in graphene layers," *J. Phys.: Condens. Matter.* **25**, 215301 (2013).
- [70] Y. Fan, Z. Wei, H. Li, H. Chen, and C. M. Soukoulis, "Photonic band gap of a graphene-embedded quarter-wave stack," *Phys. Rev. B* **88**, 241403 (2013).
- [71] J. Si and C. Sun, "On the optical performance of composite structures of graphene and photonic crystals at infrared wavelengths," *J. Appl. Phys.* **122**, 133104 (2017).
- [72] H. F. Jones, M. Kulishov, "An angle on invisibility," *arXiv:1506.02436* (2015).
- [73] B. Wunsch, T. Stauber, F. Sols and F. Guinea, "Dynamical polarization of graphene at finite doping," *New J. of Phys.* **8**, 318 (2006).
- [74] E. H. Hwang and S. Das Sarma, "Dielectric function, screening, and plasmons in two-dimensional graphene," *Phys. Rev. B* **75**, 205418 (2007).
- [75] L. A. Falkovsky, "Optical properties of graphene and IV-VI semiconductors," *Physics-Uspekhi* **51**, 887 (2008).
- [76] A. Mostafazadeh, "Optical spectral singularities as threshold resonances," *Phys. Rev. A* **83**, 045801 (2011).
- [77] T. Y. Fan, J. L. Daneu, "Thermal coefficients of the optical path length and refractive index in YAG," *App. Optics* **37**, 1635 (1998).
- [78] M. Bertolotti, V. Bogdanov, A. Ferrari, A. Jascow, N. Nazorova, A. Pikhtin, and L. Schirone, "Temperature dependence of the refractive index in semiconductors," *J. Opt. Soc. Am. B* **7**, 918 (1990).
- [79] S. A. Maier, *Plasmonics: Fundamentals and Applications*, Springer Science+Business Media LLC, New York 2007.